Relevance of pinning, nucleation, and interaction in nanograined epitaxial hard magnetic $SmCo_5$ films

A. Singh,* V. Neu,† S. Fähler, K. Nenkov, L. Schultz, and B. Holzapfel
IFW Dresden, Institute for Metallic Materials, P.O. Box 270116, D-01171 Dresden, Germany
(Received 15 December 2008; revised manuscript received 8 May 2009; published 3 June 2009)

Epitaxial growth of $SmCo_5$ films on substrates with two different symmetries was used to tailor film texture. A geometry where the easy axes of all grains are aligned in parallel is compared with a geometry where two sets of grains have a perpendicular alignment. For these two types of films with well defined nanoscaled microstructures, the role of pinning, nucleation, and intergrain interactions for the key permanent magnetic properties, namely, coercivity and remanence, is studied. The angular dependency of switching field and remanence reveals that the depinning of domain walls rules the magnetization reversal. In addition, these measurements indicate that the magnetization processes occur independently within each set of perpendicularly aligned grains. Although a large positive δJ indicates strong intergrain interactions, remanence enhancement is absent in both samples. An analysis of the irreversible susceptibility during the magnetizing and demagnetizing processes gives a complete picture of the relevant processes, and shows that both pinning and nucleation of domains are involved.

DOI: 10.1103/PhysRevB.79.214401 PACS number(s): 75.50.Ww, 75.70.Ak, 75.50.Tt, 81.15.Fg

I. INTRODUCTION

In order to tailor the response of a magnetic material to an external magnetic field, a sound understanding of the underlying magnetization processes in the studied system is required. For permanent magnet materials, which increasingly gain importance in thin-film form, this central question culminates in understanding the origin of coercivity. Consequently the magnetization reversal or coercivity mechanism has been thoroughly investigated for several hard magnetic thin films.[1–6] As an extrinsic property the coercivity and its mechanism depends on the details of the microstructure and its origin can only be answered for each individual case.

In this paper, the study of the coercivity mechanism in epitaxial nanocrystalline $SmCo_5$ (Ref. 6) has been extended to films with perpendicular orientation of the easy magnetization direction of neighboring grains. Furthermore it includes various angle dependent measurements and irreversible susceptibility data in the magnetizing and the demagnetizing branches. In order to facilitate a consistent interpretation of these measurements the basic principles of magnetization reversal in small particle systems and in extended films are shortly reviewed, focusing especially on the interpretation of susceptibility measurements.

Magnetization reversal follows the basics of micromagnetism and can be classified into several broad categories.[7–9] In the simplest case of isolated (noninteracting) small particles, whose sizes are below the single domain particle size, the magnetization reversal is expected to follow the coherent rotation process described by Stoner and Wohlfarth.[10] When all particles exhibit the same uniaxial anisotropy, the reversal is simply governed by the easy axis distribution across the particle ensemble. Deviations from the interaction-free scenario, both due to magnetostatic and direct exchange, leading to significant modifications of the magnetization behavior. In these small grained ensembles, interactions manifest themselves in an asymmetry between the magnetizing and the demagnetizing processes, and are often probed by a δJ analysis, which balances the remanence magnetization as a function of the formerly applied field starting from the thermally demagnetized (magnetizing branch J_R^M) and the saturated (demagnetizing branch J_R^D) states, respectively.[11,12] Especially intergrain exchange coupling has been extensively investigated with the aim of enhancing remanence and therefore improving the energy density $(BH)_{\max}$ above the Stoner-Wohlfarth limit for isotropic magnets by reducing the grain size down to a few tens of the exchange-correlation length $d=\sqrt{A/K}$.[13–17] This formula describes the competition of exchange coupling constant (A) favoring a parallel alignment of neighboring spins with the magnetocrystalline anisotropy constant (K) favoring an alignment of spins with respect to the crystal lattice.

For large grained samples the Stoner-Wohlfarth approach is no longer applicable. As is known, e.g., in the well studied sintered $Nd_2Fe_{14}B$-, $SmCo_5$-, or Sm_2Co_{17}-based magnets, inhomogeneous magnetization states or the formation of reversed domains within a grain during the demagnetizing process are no longer prohibited and the coercivity is determined by the ease with which reversed domains can nucleate and expand. Based on this, magnets can be classified in a simplified way into nucleation- and pinning-type magnets.[8,18,19] In a nucleation-type magnet, domain-wall movement is relatively easy but the magnetization reversal from the saturated state first requires the nucleation of a reversed domain which occurs at high fields. On the other hand, in a pinning-type magnet the formation of reversed nuclei costs less energy than the depinning or expansion of these reversed domains. Therefore the fields required for the depinning of domain walls from defects determine the coercivity. In such multidomain magnets the Stoner-Wohlfarth criterion is necessarily violated and δJ cannot be expected to be zero due to the difference in the domain configuration of the thermally demagnetized and saturated states. Domains present in the demagnetized state can be driven out from the system, and thereby lead to an increased J_R^M, in relatively low fields. In contrast reversal from the saturated state requires

the application of a large nucleation field. Thus large positive δI are typically observed for a high coercive nucleation-type magnet, such as sintered large grained Nd-Fe-B.[20–22] In pinning-type magnets the effect of the coercivity mechanism on the results of a δI analysis is less well studied. The irreversible susceptibility calculated from the remanence analysis performed in the magnetizing branch is often identified with the pinning field distribution within the magnet.[23,24] Assuming that the same pinning distribution also governs the demagnetizing process leads to the prediction of a vanishing δI (Ref. 25) but this is often in contradiction with experimental observations.[26]

The classification of the coercivity mechanism into small particle switching, pinning, and nucleation complicates further when the magnetic system consists of small distinguishable entities, e.g., grains with individual local easy axis orientation, which are, however, so well coupled that they form areas of roughly homogeneous magnetization larger than the size of the underlying entities and result in a special type of domain. Such collective magnetization patterns have been named "interaction domains" when they originate from magnetostatic coupling[27,28] but the term is equally appropriate for coupling of neighboring grains by direct exchange.[29] Whether and to which extent such interaction domains can be classified to follow a pinning- or nucleation-type coercivity mechanism is not altogether well studied but presents a key question in today's nanoscaled and nanostructured magnetic materials.

Here, we clarify the relevance of nucleation, pinning, and exchange interactions on the coercivity mechanism in epitaxial $SmCo_5$ thin films. For this, we compare the angle dependent hysteresis and irreversible susceptibility in the magnetizing and the demagnetizing branches of two nanoscaled $SmCo_5$ films with two distinctly different epitaxial textures. The data can be convincingly described in the framework of a pinning controlled coercivity mechanism. In extension to the previous study,[6] however, the susceptibility data and the angle dependent measurements require a modification of the pinning picture, in which the contribution of nucleation and the nanocrystalline microstructure play a significant role, and hence cannot be ignored.

II. SAMPLE PREPARATION, MICROSTRUCTURE, AND MAGNETIC MEASUREMENTS

As described in detail earlier,[30,31] $SmCo_5$ films with a thickness of 50 nm were deposited using pulsed laser deposition from elemental targets in a ultrahigh-vacuum deposition system (base pressure of 2×10^{-9} mbar) on MgO(001) and MgO(110) single-crystal substrates. From the pioneering experiments of Fullerton *et al.*,[32] it is known that Sm_2Co_7 grows epitaxially on these two different substrates. While in both cases the magnetic easy axis is aligned in plane, the arrangement within the film plane differs. The twofolded surface symmetry of the Cr(211) buffer on the MgO(110) substrate allows for a unique alignment of the easy axis, whereas the fourfolded surface symmetry of the Cr(001) buffer on MgO(001) substrates results in the growth of two sets of Sm-Co grains having their easy axes perpendicular to each

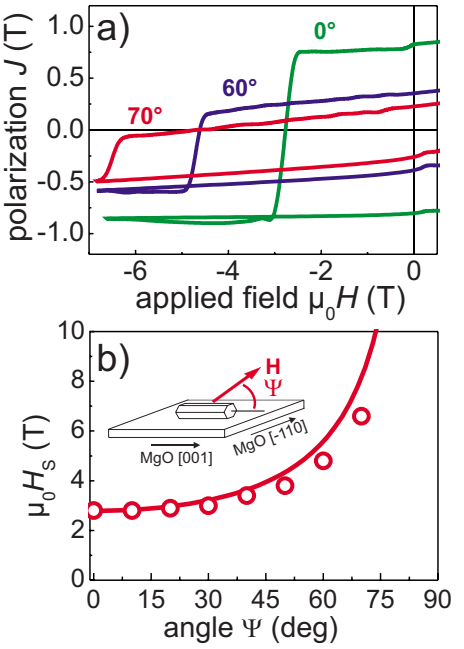

FIG. 1. (Color online) (a) Demagnetizing branch for a $SmCo_5$ film on MgO(110) single-crystal substrate at varying angles $\Psi=0°$, 60°, and 70°. (b) Switching field (open circles) and calculated inverse cos dependence (solid line) as a function of the out-of-plane angle Ψ between the applied field and the in-plane *c* axis.

other. In our recent work[30,31] we show that identical growth is also possible for the $SmCo_5$ phase, exhibiting a favorable higher anisotropy and saturation polarization compared to the Sm_2Co_7 phase examined by Fullerton *et al.* The two $SmCo_5$ geometries on MgO(110) and MgO(001) substrates are sketched in the insets of Figs. 1 and 2, and in the following are described as single-variant [grown on MgO(110)] and two-variant states [grown on MgO(001)]. Both the single-variant and the two-variant cases are model systems with well defined geometries, with only small-angle grain boundaries existing in the former case, while the latter exhibits a large number of 90° grain boundaries. Both types of films are smooth, continuous, and possess sharp interfaces between the Cr buffer, the $SmCo_5$ layer, and the Cr cover layer without visible interdiffusion.[30,33] The Sm-Co grains are about 50–100 nm in size and grow in a columnar fashion spanning the entire film thickness [as found from previous transmission electron microscopy investigations[34]]. Local magnetic force microscopy (MFM) observations indicate that the domain size in these samples can be as small as 100 nm, indicating that the grains are essentially single domain entities.[35,36]

Magnetic characterization of the samples was performed in a superconducting quantum interference device magnetic property measurement system with the highest applied field of 7 T and the possibility to rotate the sample continuously in the field, and in a physical property measurement system vibrating sample magnetometer (PPMS-VSM) with an applied field up to 9 T. Hysteresis curves were measured at different angles Φ between the in-plane easy axis and in-plane applied field, and Ψ between the in-plane easy axis and an applied field tilted toward the film normal. For the two-

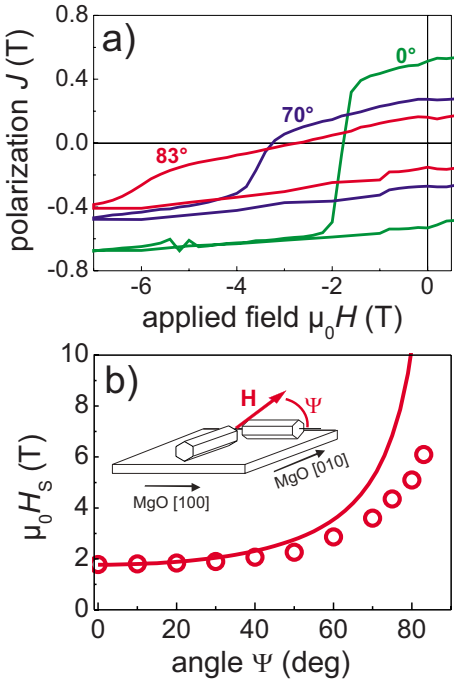

FIG. 2. (Color online) (a) Demagnetizing branches of a $SmCo_5$ film on MgO(001) single-crystal substrate at varying angles $\Psi = 0°$, 70°, and 83°. (b) Switching field (open circles) and calculated inverse cos dependence (solid line) as a function of the out-of-plane angle Ψ between the applied field and the in-plane c axis of one of the grain variants.

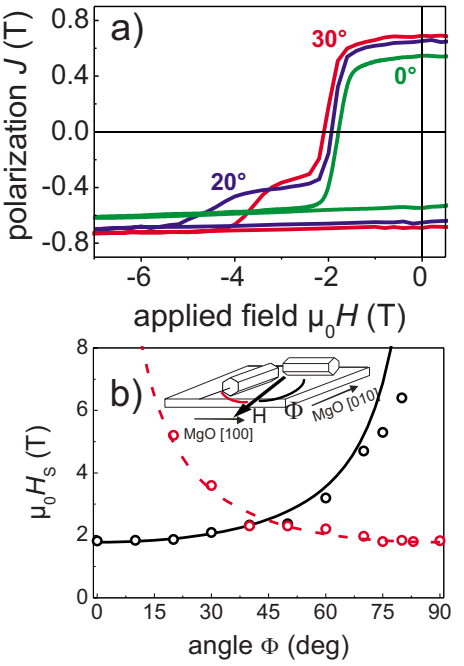

FIG. 3. (Color online) (a) Demagnetizing branches of a $SmCo_5$ film on MgO(001) single-crystal substrate at varying angle $\Phi = 0°$, 20°, and 30°. (b) Switching fields (open circles) and calculated inverse cos dependence (solid line) as a function of the in-plane angle Φ between the applied field and the in-plane c axis of one of the grain variants together with the inverse $\cos(90° - \Phi)$ dependence (dashed line) predicting the switching field in the perpendicular grain variant.

variant case, where two equally probable but perpendicular orientations of the easy axis occur, the angle Φ and Ψ refer to one of these orientations. Pictorial representations of angles Ψ and Φ are given in the insets of Figs. 2 and 3. Recoil loop measurements were performed on the samples in small steps of 0.25 T up to maximum applied fields of 9 T with the PPMS-VSM. For the following experiments, two films with optimized properties were selected, i.e., both films exhibit a coercivity of more than 3 T, and also correspondingly high remanences of 0.94 T for the single-variant state and 0.71 T for the two-variant state, reflecting the difference in the easy axis distribution.[30,31]

III. RESULTS AND DISCUSSION

A. Angular dependent hysteresis measurements

The coercivity mechanism of the single-variant film was analyzed by a micromagnetic analysis, angular dependent measurements, and MFM in a previous study.[6] In that attempt to describe the magnetization processes—which will be partly modified here—it was suggested that the coercivity in these films is controlled by pinning, and that domain nucleation can be neglected. The strongest argument came from angular dependent hysteresis measurements, in which the switching fields followed Kondorsky's 1/cos dependence.[37] This dependence describes a magnetization reversal by depinning of domain walls in a uniaxial system where only 180° domain walls are present. For a comparison with the more complex two-variant state, angle dependent hystereses on the single-variant sample are now measured with an increased field component perpendicular to the film plane (Fig. 1). For the single-variant sample, the hysteresis measured along the easy axis is square shaped and shows a sharp magnetization transition at the switching field $\mu_0 H_S$, defined as the maximum of the irreversible susceptibility. When applying the field under an angle $\Psi = 60°$ with respect to the film plane, the hysteresis is not square shaped anymore but a certain slope is observed due to reversible rotation of magnetization toward the direction of applied field. As for the 0° measurement, irreversible magnetization switching is observed as a sharp decrease in polarization which occurs at higher negative fields. With increased measurement angle $\Psi = 70°$, both of these observations (increased slope and larger switching field) become more pronounced. However, compared to the 60° measurement the switching field H_S increases whereas the coercivity value H_C remains constant. This is understood from the fact that the coercivity H_C is defined as the field at which the magnetization vanishes in the sample, and therefore has contributions from both the reversible and irreversible processes. Hence, the switching field H_S is a more appropriate sample property to define irreversible magnetization switching. For 90° an almost completely closed hysteresis is observed, as only reversible rotation of magnetization toward the external field occurs (not shown here). The summary of H_S [Fig. 1(b)] reveals a strong increase with angle. Values fit well with an inverse cosine dependence (solid line). Following the concept of

Kondorsky[37] and as discussed extensively recently,[6] this indicates an efficient pinning of domain walls as the origin of coercivity. The small deviation from the 1/cos dependence is caused by the already discussed rotational processes, which also modify the energy of the domain wall and hence the depinning field. Such effects are discussed, e.g., by Schuhmacher[38] and scale with the ratio of switching field to anisotropy field. Consequently the deviations increase for higher angles.

Angular dependent measurements performed in a similar fashion with the field applied at an out-of-plane angle on a 150-nm-thick two-variant $SmCo_5$ sample are summarized in Fig. 2. The in-plane field component is chosen to be parallel to one grain variant, so that with varying Ψ (the angle between the easy axis of one variant and the field), the field is always perpendicular to the easy axis of the second variant. Thus, the magnetization rotation within the second variant contributes to a constant slope, visible already for $\Psi=0°$, in contrast to the rectangular loop of the single-variant sample. Except for this additional slope, the hystereses measured for the different angles Ψ are similar to the single-variant case. With increasing Ψ from 0° to 70° and further to 83°, the switching field increases and the remanent magnetization decreases [Fig. 2(a)]. The angle dependence of all measurements for varying Ψ on the two-variant sample is summarized in Fig. 2(b). A similar increase in H_S with angle as for the single-variant case is observed; however a fit with $1/\cos\Psi$ is not as good as for the single-variant sample.

For the two-variant sample hysteresis measurements were also performed with varying in-plane angle Φ (Fig. 3). Since the field is applied in the film plane at an angle Φ with respect to one of the easy axes, the other variant experiences the applied field at the complementary angle of $(90°-\Phi)$. The hysteresis for $\Phi=0°$, which is parallel to the easy axis of one variant and perpendicular to the other, exhibits one sharply defined switching field and the expected additional slope [Fig. 3(a)]. As shown exemplarily for $\Phi=20°$ and 30°, a second switching process is observed at higher negative fields for all nonsymmetric orientation ($\Phi\neq 0°$, 45°, and 90°). This suggests that the magnetization in the complementary variant is not only rotating but also switching. The switching occurs at two well defined fields which are summarized in Fig. 3(b) and are attributed to the magnetization reversal in the respective variants. For Φ close to 45° where a symmetric situation exists for both the variants, the switching fields cannot be separated. Both the switching fields increase with increasing angle and can be fitted well with a 1/cos dependence. This demonstrates that the magnetization reversal in both variants appears independent of each other, and is determined by the depinning and expansion of domain walls.

Up to this point, the results seem to be consistent and straightforward: for the two-variant sample there are two independent sets of grains, and switching in each one of them is controlled by pinning. However, variants are connected and form a continuous film. As the variant size is about 50–100 nm, interaction between different variants might be necessary to consider. An exchange interaction in the system is expected to result in remanence enhancement and often a positive deviation of δJ is interpreted as a kind of proof.

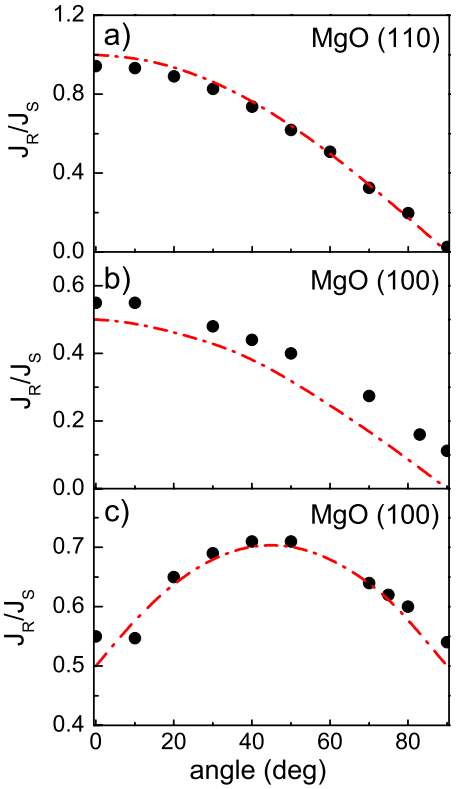

FIG. 4. (Color online) (a) Angular variation in remanent polarization J_R (full circles) for the single-variant film and the expected cos Ψ dependence (dotted line). (b) Angular dependence measured for the two-variant sample on MgO(001) and the expected 0.5 $\times$cos Ψ dependence. (c) Angular variation in remanent polarization J_R (full circles) for the two-variant sample as a function of the in-plane angle Φ together with the predicted Stoner-Wohlfarth $(J_S/2)(\cos\Phi+\sin\Phi)$ dependence (dotted line).

Remanent polarization for the single-variant and the two-variant samples were extracted from the angular dependent hysteresis measurements and are summarized in Fig. 4. The normalized remanent polarization J_R/J_S for increasing angle Ψ on the single-variant sample [Fig. 4(a)] decreases with increasing angle Ψ and shows a cos Ψ dependence (dashed line), indicating that in the remanent state the magnetization lies along the easy axis and only the projection J_S cos Ψ of the saturation polarization is contributing to the measurement along the previous field direction. Similar measurements on the two-variant film reveal a similar decrease in polarization with increasing angle Ψ [Fig. 4(b)]. In comparison to the single-variant case the remanent values reach only half of the saturation magnetization (dashed line) since only half of the variants can contribute. When the angle is varied in the film plane from one variant to another, a maximum of J_R/J_S at 45° is obtained [Fig. 4(c)]. This however is no indication of remanence enhancement by exchange coupling, but just a direct consequence of the two-variant geometry. In this geometry, the projection of both variants onto the field direction contributes to the remanence. Experimental data follow the expected $(J_S/2)(\cos\Phi+\sin\Phi)$ dependence (dashed line). It is the more general case of the measurement at $\Phi=45°$, which was published earlier for a different sample.[30]

We can therefore conclude that for all the three measurement configurations the normalized remanent polarization behaves in accordance with the Stoner-Wohlfarth prediction and we do not observe any hint of remanence enhancement. This is obvious for the single-variant case, where due to the epitaxial growth all the easy axes and therefore the magnetic moment is already aligned along one single direction in the remanent state. In the two-variant sample on the other hand, magnetization cannot change abruptly across the grain boundary from one easy axis orientation to the 90° neighbor as the term for the exchange energy $E_{ex}=A\cdot\nabla[\vec{m}(\vec{r})]^2$ requires a continuous rotation of the magnetic moments. These moments can in principle contribute to a remanence enhancement above the geometrical limit of the Stoner-Wohlfarth model. The experimental absence of remanence enhancement is in accordance with numerical estimates based on the length ratio D/d, D being the average grain diameter and d being the exchange-correlation length. For a reduced grain size of $D/d>100$, as in the studied system, calculations predict a remanence enhancement of less than 3%.[39] Although these calculations describe an ensemble with isotropic in-plane easy axis distribution, a similarly low value is expected for the present texture.

B. Irreversible susceptibilities in the magnetizing and demagnetizing processes

Although remanence enhancement is neither expected nor observed, the nanocrystalline microstructure with small connected grains may still have an influence on the overall magnetization behavior through intergrain exchange coupling. Instead of simply looking for the remanence after full saturation, a δJ analysis probes the irreversible switching processes in the magnetizing and demagnetizing branches of the hysteresis. This kind of measurement can therefore be used to analyze the effect of interactions on the magnetization reversal mechanism. Starting from the as deposited thermally demagnetized state, the sample is subjected to a certain positive magnetizing field H_{app} applied parallel to (one of) the easy axis, which was then reduced to zero, and the remanent magnetization J_R^M is measured (Fig. 5). (The vanishing demagnetizing factor in the in-plane geometry allows identifying of the applied field with the internal field, which has to be considered in a δJ analysis.) This process is repeated with increasing applied field (up to 9 T), resulting in the remanent values $J_R^M(H_{app})$. As a next step the demagnetizing process was analyzed by repeating these measurements with negative demagnetizing fields H_{app} which gives $J_R^D(H_{app})$. For a system of noninteracting ellipsoidal single domain particles with uniaxial anisotropy, the following equation should hold:[10]

$$J_R^D(H_{app})/J_R^\infty = 1 - 2J_R^M(H_{app})/J_R^\infty. \quad (1)$$

$J_R^\infty=J_R^M(9\ \mathrm{T})$ is the maximum remanence after applying a 9 T field. δJ is the deviation from this equality which arises from violation of any of the listed conditions, especially the noninteraction and the single domain character. In small grained samples with uniaxial anisotropy a positive δJ is commonly interpreted as a consequence of exchange coupling, whereas a negative value is interpreted as magnetostatic interactions.[40,41] δJ plots for both samples are presented in Fig. 6 and show positive deviations. The two-variant film on MgO(001) substrate shows a moderate positive δJ with values which lie in the range of what is reported for nanocrystalline hard magnetic thin films.[26,42] Although the effect of coupling on remanence enhancement is negligible due to the large grain size, obviously the direct intergrain exchange interactions modify the magnetization reversal in this ensemble of coupled single domain grains. In case of the single-variant film the positive δJ is even more pronounced and reaches the maximum theoretical value of 2. When considering this film as an ensemble of nanocrystalline grains, the positive δJ can be understood as the effect of exchange coupling to the well aligned neighboring grains. This stabilizes the magnetization of an individual grain against reversal when starting from the saturated state. When starting from the thermally demagnetized state, exchange coupling averages out due to the presence of neighboring grains with antiparallel orientation of their magnetic moments. In this sample grains are only separated by small-angle grain boundaries and the coupling is apparently so strong that it justifies the view that the coer-

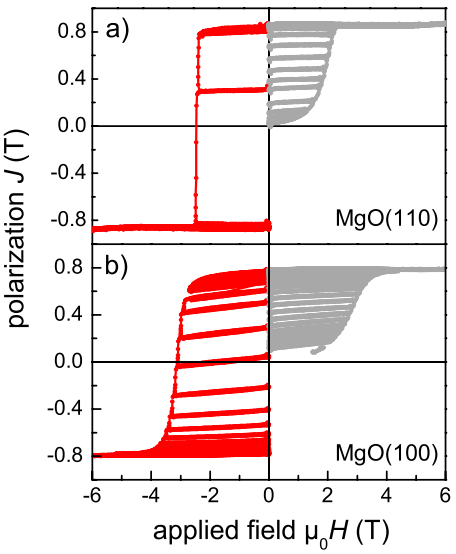

FIG. 5. (Color online) Measured recoil loops for $SmCo_5$ films on (a) MgO(110) and (b) MgO(001) substrates, respectively.

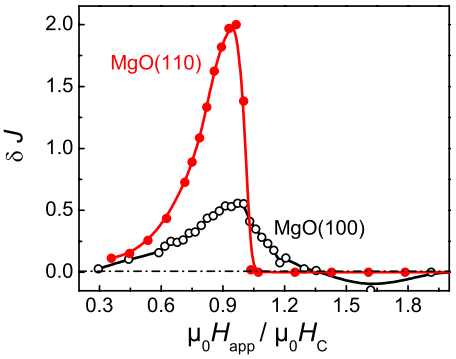

FIG. 6. (Color online) δJ plots for $SmCo_5$ films on MgO(110) and MgO(001) substrates. Measurements were performed with the applied field parallel to (one of) the easy axis.

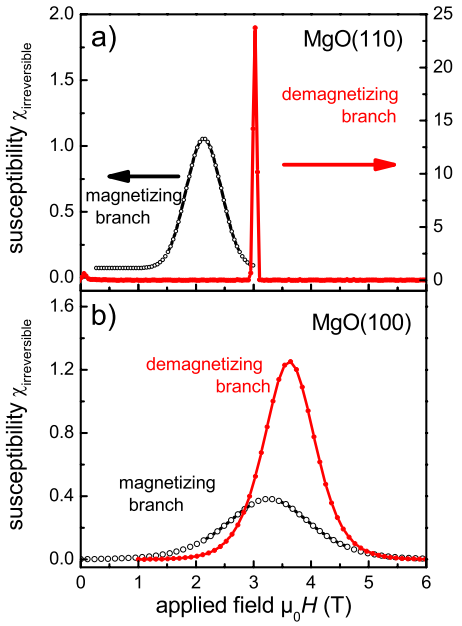

FIG. 7. (Color online) (a) Irreversible susceptibility for the single-variant film on MgO(110) in the magnetization and demagnetization branches. (b) Irreversible susceptibility for the two-variant sample on MgO(001) in the magnetization and demagnetization branches.

civity is determined by the depinning of 180° domain walls.

In the following we will develop a model to explain both, angle dependent switching fields and recoil loops for both types of samples. For this we discuss the individual irreversible susceptibilities in the magnetizing and the demagnetizing branches of the hysteresis in more detail.

For the single-variant film [Fig. 7(a)] the irreversible susceptibility distribution during the magnetizing process $\chi_{\mathrm{irr}}^{M} = \partial J_R^M / \partial(\mu_0 H_{\mathrm{app}})$ shows a maximum at $\mu_0 H_m = 2.1$ T. This maximum is quite broad [full width at half maximum $\Delta(\mu_0 H) = 0.79$ T] as compared to the demagnetizing process, for which a very sharp maximum [$\Delta(\mu_0 H) = 0.10$ T] occurs at the coercivity of 3 T. To understand these differences one needs to consider the different domain configurations at the beginning of both processes. In the thermally demagnetized state, we reported on a quite small domain pattern, which is observed by magnetic force microscopy[35] and may be considered as a large number of nuclei in the order of 10^{10} cm^{-2}. In the magnetizing process they grow by expanding into the neighboring not yet reversed domains. The broad irreversible susceptibility peak thereby suggests a broad distribution of pinning fields. The density of strong pinning sites can also be estimated from magnetic force microscopy measurements and amounts to a likewise high number of 10^{10} cm^{-2}.[6] A different starting situation exists for the demagnetization process where magnetization reversal sets in from a single domain state. Let us first assume that the present system is a simple pinning dominated magnet in which the nucleation of a reverse domain is relatively easy. Hence small nuclei could form at low fields at all defects within the sample. These nuclei can then expand across the next-nearest pinning site once the corresponding pinning field is exceeded. This pinning field distribution therefore should result in an irreversible susceptibility $\chi_{\mathrm{irr}}^{D} = \partial J_R^D / \partial(\mu_0 H_{\mathrm{app}})$ qualitatively comparable to that of the magnetizing branch, χ_{irr}^{M}, as briefly discussed in Sec. I. This is obviously not the case in our present system where magnetization reversal occurs at a well defined field and finishes in a very narrow field interval. The observed difference between χ_{irr}^{M} and χ_{irr}^{D} hints for domain nucleation. Indeed a large well defined nucleation field which needs to be overcome to initiate the magnetization reversal could explain the observation. If the nucleation field lies above the largest pinning field, domain expansion cannot be hindered by the present pinning sites. As a consequence the broad pinning field distribution measured by the magnetizing branch is not probed via χ_{irr}^{D}.

The strong coincidence between the peak position in χ_{irr}^{D} and the largest pining field deduced from χ_{irr}^{M} leads us to an altogether new hypothesis. We suggest that the nucleation in these films may occur already at relatively low fields; however, the density of these nucleation sites is well below the density of strong pinning centers. Due to this, the few nuclei that exist can grow already at low fields by overcoming weaker pinning sites but their contribution to the overall magnetization is negligible. Only when the applied field exceeds the strongest pinning field does domain expansion lead to an abrupt magnetization reversal which is again governed by the strength and density of the strong pinning sites. The picture reconciles the large discrepancy of χ_{irr}^{D} and χ_{irr}^{M} which is better known for nucleation-type magnets and the observed angular dependence of coercivity (valid for pinning-type magnets), and the obvious presence of pinning sites. We thus conclude that these $SmCo_5$ films show a pinning dominated magnetization reversal; however with two additional important conditions. First, to probe the full pinning field distribution as measured in χ_{irr}^{M}, the initial domain structure in the thermally demagnetized state has to be exceptionally small scaled. In the present study, this is the result of the nanocrystalline microstructure which forces the domain size in the demagnetized state to be considerably smaller than the single domain particle limit (800 nm). The second condition is that nucleation sites with low nucleation fields are present only in very low density. Consequently, when avoiding the large number of nucleation centers represented by the initial nanoscaled domain structure, the switching field can be shifted above the most prevalent pinning field. This explains the very sharp demagnetizing susceptibility in contrast to the broad magnetizing susceptibility, in a way that the magnetizing susceptibility represents the entire range of pinning strengths available, whereas in the demagnetizing process only the most efficient pinning defects are active in controlling magnetizing reversal. Hence, these susceptibility measurements show that both nucleation and pinning are involved during magnetization reversal.

The two-variant films grown on MgO(001) can be used to test this concept. The irreversible susceptibility χ_{irr}^{M} is qualitatively similar but broader [$\Delta(\mu_0 H) = 1.66$ T] and shifted to higher field values ($\mu_0 H_m = 3.26$ T) as compared to the single-variant sample. In contrast to the single-variant sample, the irreversible susceptibility for the magnetizing χ_{irr}^{M} and demagnetizing χ_{irr}^{D} cases are qualitatively very similar. χ_{irr}^{D} is only slightly sharper [$\Delta(\mu_0 H) = 1.02$ T], is hardly

shifted ($\mu_0 H_m = 3.64$ T), and differs from χ_{irr}^M mainly by the expected factor of two in the enclosed area. When considering χ_{irr}^M as a pinning field distribution, the two-variant sample obviously possesses the stronger pinning sites. The similarity of χ_{irr}^M and χ_{irr}^D can be understood from the same concept developed to describe the difference of both susceptibilities for the single-variant film. In the virgin state the sample develops a likewise fine scaled domain pattern as the single-variant sample;[36] however, from the angular dependent hysteresis (Fig. 3) one can conclude that an applied field of 9 T is not sufficient to switch the magnetization in variants having their easy axis perpendicular to the field. Hence the virgin domain pattern in these variants should remain mostly unaffected even after saturation. Following the above described concept this domain pattern promotes domain-wall movement for those variants having their easy axis parallel to the applied field. The high number of nuclei present in the form of existing domains in both states can explain why the irreversible susceptibility is broad for both the magnetizing and demagnetizing cases, and why their maxima differ only by 12% in comparison to a 43% change in the single-variant sample. The weighted difference of both curves, which results in δI, is thus significantly smaller compared to the single-variant case. As for the single-variant case the remaining difference can be attributed to annihilation of domains within each variant during the magnetizing process. This suggests that pinning centers are also present within the variant having the easy axis parallel to the field, and indicates that the density of pinning sites is higher than the density of variant boundaries.

The present integral experiments do not reveal the microscopic nature of the defects and their ability to act as pinning or nucleation sites. We judge, however, the defect distribution suggested to explain the magnetic behavior as very reasonable for the studied films. The samples consist of numerous small grains where the grain boundaries necessarily present planar structural defects with a dimension of a few nanometers and a very fine spacing of about 100 nm. Depending on the texture of the film, these are only small-angle grain boundaries with misorientations of up to 5° (Ref. 6) or a mix of about 90° angle grain boundaries and small-angle grain boundaries. The latter exist only in the two-variant sample if the variant size is larger than the grain size. Additionally, stacking faults along the c axis are identified in an earlier study on sputtered Sm_2Co_7 (Ref. 43) and may also be present in these laser deposited $SmCo_5$ films. These stacking faults appear on an even smaller spacing of below 10 nm. From both the grain boundaries and the stacking faults, pinning of domain walls can be expected, as the length scale of reduced crystallographic order and therefore the profile with modified intrinsic parameters matches well with the exchange-correlation length of about 1 nm in $SmCo_5$. The pinning field distribution may originate from the dependence of pinning strength on the details of the disturbed region as, e.g., the misorientation angle of neighboring grains. The latter dependency may also explain the larger pinning strength for the samples containing 90° grain boundaries. Defect size does not only affect pinning efficiency but also the probability for nucleation. These effects however exhibit a different size dependence.[44] Our observations suggest a high number of small defects where the nucleation field is higher than the pinning field but a low number of large defects having a small nucleation field.

IV. CONCLUSIONS

Epitaxial growth is used to prepare nanoscaled $SmCo_5$ films with two well defined geometries in order to examine the role of exchange coupling, pinning, and nucleation. The angular dependent measurements of the switching field show that the depinning of domain walls rules the magnetization reversal in these films. Positive δI values are recorded in both types of samples even up to a maximum theoretical value of 2 without observing any remanence enhancement. The analysis of the irreversible susceptibility in the magnetizing and demagnetizing processes reveals an asymmetric behavior, which is explained by a high density of nuclei in the form of reversed domains in the virgin state and reduced existence when approaching coercivity from the saturated state. The positive δI is explained by the inability of the few existing nuclei in the saturated state to expand since they are hindered by the high density of strong pinning sites. The density of such nucleation sites is expected to be well below 10^{10} cm^{-2}. Nevertheless, the present experiments show that both pinning and nucleation have to be considered during the switching process.

ACKNOWLEDGMENTS

The authors would like to acknowledge the support of DFG for funding the project via SFB 463 "Rare Earth Transition Metal Compounds—Structure, Magnetism and Transport."

*aarti.asingh@gmail.com
†v.neu@ifw-dresden.de

[1] K. Schnitzke, L. Schultz, J. Wecker, and M. Katter, Appl. Phys. Lett. **57**, 2853 (1990).
[2] D. Elbaz, D. Givord, S. Hirosawa, F. Missell, and M. Rossignol, J. Appl. Phys. **69**, 5492 (1991).
[3] E. Bonet, W. Wernsdorfer, B. Barbara, A. Benoit, D. Mailly, and A. Thiaville, Phys. Rev. Lett. **83**, 4188 (1999).
[4] U. Hannemann, S. Fähler, V. Neu, B. Holzapfel, and L. Schultz, Appl. Phys. Lett. **82**, 3710 (2003).
[5] S. L. Chen, W. Liu, and Z. D. Zhang, Phys. Rev. B **72**, 224419 (2005).
[6] A. Singh, V. Neu, S. Fähler, K. Nenkov, L. Schultz, and B. Holzapfel, Phys. Rev. B **77**, 104443 (2008).
[7] J. D. Livingston, J. Appl. Phys. **52**, 2544 (1981).
[8] H. Kronmüller, Phys. Status Solidi **130**, 197 (1985).

[9] D. Givord, M. Rossignol, and V. M. T. S. Barthem, J. Magn. Magn. Mater. **258-259**, 1 (2003).
[10] E. C. Stoner and E. P. Wohlfarth, Philos. Trans. R. Soc. London, Ser. A **240**, 599 (1948).
[11] O. Henkel, Phys. Status Solidi **7**, 919 (1964).
[12] K. C. Schuermann, J. D. Dutson, S. Z. Wu, S. D. Harkness, B. Valcu, H.-J. Richter, R. W. Chantrell, and K. O'Grady, J. Appl. Phys. **99**, 08Q904 (2006).
[13] R. W. McCallum, A. M. Kadin, G. B. Clemente, and J. E. Keem, J. Appl. Phys. **61**, 3577 (1987).
[14] H. A. Davies, J. Magn. Magn. Mater. **157-158**, 11 (1996).
[15] V. Neu, L. Schultz, and H.-D. Bauer, Nanostruct. Mater. **12**, 769 (1999).
[16] K. C. Liu, J. D. Zhang, S. Z. Liu, S. D. Chen, B. He, H.-J. Liu, R. W. Sun, and K. Sellmyer, Adv. Mater. **14**, 1832 (2002).
[17] W. Scholz, T. Schrefl, J. Fidler, T. Matthias, D. Suess, and V. Tsiantos, IEEE Trans. Magn. **39**, 2920 (2003).
[18] H. Kronmüller, K. D. Durst, and G. Martinek, J. Magn. Magn. Mater. **69**, 149 (1987).
[19] D. Givord, P. Tenaud, and T. Viadieu, J. Magn. Magn. Mater. **72**, 247 (1988).
[20] K.-H. Müller, D. Eckert, A. Handstein, and P. Nothnagel, J. Magn. Magn. Mater. **104-107**, 1173 (1992).
[21] F. Cebollada, M. F. Rossignol, D. Givord, V. Villas-Boas, and J. M. Gonzalez, Phys. Rev. B **52**, 13511 (1995).
[22] R. W. Gao, D. H. Zhang, W. Li, X. M. Li, and J. C. Zhang, J. Magn. Magn. Mater. **208**, 239 (2000).
[23] J. F. Liu and G. C. Hadjipanayis, J. Magn. Magn. Mater. **195**, 620 (1999).
[24] R. Varga, P. Vojtanik, and R. Andrejco, Phys. Status Solidi **193**, 103 (2002).
[25] X. Du, H. Zhang, C. Rong, J. Zhang, S. Zhang, B. Shen, Y. Yana, and H. Jina, J. Magn. Magn. Mater. **281**, 255 (2004).
[26] C. Prados and G. C. Hadjipanayis, Appl. Phys. Lett. **74**, 430 (1999).
[27] A. Hubert and R. Schäfer, *Magnetic Domains* (Springer-Verlag, Berlin, 1998).
[28] K. Khlopkov, O. Gutfleisch, R. Schäfer, D. Hinz, K.-H. Müller, and L. Schultz, J. Magn. Magn. Mater. **272-276**, E1937 (2004).
[29] R. Chen, J. Wang, H. Zhang, B. Shen, and A. Yan, J. Phys. D **40**, 4391 (2007).
[30] A. Singh, V. Neu, R. Tamm, K. Rao, S. Fähler, W. Skrotzki, L. Schultz, and B. Holzapfel, Appl. Phys. Lett. **87**, 072505 (2005).
[31] A. Singh, V. Neu, R. Tamm, K. Rao, S. Fähler, W. Skrotzki, L. Schultz, and B. Holzapfel, J. Appl. Phys. **99**, 08E917 (2006).
[32] E. E. Fullerton, C. H. Sowers, J. P. Pearson, S. D. Bader, X. Z. Zu, and D. Lederman, Appl. Phys. Lett. **69**, 2438 (1996).
[33] K. Subba Rao, Ph.D. dissertation, TU Dresden, 2006.
[34] R. Tamm, A. Singh, V. Neu, K. Subba Rao, W. Skrotzki, C.-G. Oertel, S. Leinert, S. Fähler, L. Schultz, and B. Holzapfel, Solid State Phenom. **105**, 409 (2005).
[35] V. Neu, S. Fähler, A. Singh, A. R. Kwon, A. K. Patra, U. Wolff, K. Häfner, B. Holzapfel, and L. Schultz, J. Iron Steel Res. Int. **13**, 102 (2006).
[36] U. Wolff, A. Singh, L. Schultz, and V. Neu, J. Magn. Magn. Mater. **310**, 2210 (2007).
[37] E. Kondorsky, J. Phys. (USSR) **2**, 161 (1940).
[38] F. Schumacher, J. Appl. Phys. **70**, 3184 (1991).
[39] V. Neu, A. Hubert, and L. Schultz, J. Magn. Magn. Mater. **189**, 391 (1998).
[40] I. A. Beardsley and J.-G. Zhu, IEEE Trans. Magn. **27**, 5037 (1991).
[41] H. Zhang, C. Rong, X. Du, J. Zhang, S. Zhang, and B. Shen, Appl. Phys. Lett. **82**, 4098 (2003).
[42] C. L. Harland, L. H. Lewis, Z. Chen, and B.-M. Ma, J. Magn. Magn. Mater. **271**, 53 (2004).
[43] H. Benaissa, K. M. Krishnan, E. E. Fullerton, and J. S. Jiang, IEEE Trans. Magn. **34**, 1204 (1998).
[44] H. Kronmüller, K.-D. Durst, and M. Sagawa, J. Magn. Magn. Mater. **74**, 291 (1988).